Article

High-fidelity replica molding of glassy liquid crystalline polymer microstructures

Hangbo Zhao, Jeong Jae Wie, Davor Copic, C. Ryan Oliver, Alvin Orbaek White, Sanha Kim, and Anastasios John Hart

ACS Appl. Mater. Interfaces, **Just Accepted Manuscript** • DOI: 10.1021/acsami.6b00785 • Publication Date (Web): 04 Mar 2016

High-fidelity replica molding of glassy liquid crystalline polymer microstructures

Hangbo Zhao[1, §], Jeong Jae Wie[1, 2, §], Davor Copic[3, §], C. Ryan Oliver[1], Alvin Orbaek White[1], Sanha Kim[1], A. John Hart[1,*]

[1] *Department of Mechanical Engineering, Massachusetts Institute of Technology, 77 Massachusetts Avenue, Cambridge, MA 02139, USA.*

[2] *Department of Polymer Science and Engineering, 100 Inha-ro, Nam-gu, Incheon, 402-751, Republic of Korea.*

[3] *Department of Mechanical Engineering, University of Michigan, 2350 Hayward Street, Ann Arbor, MI 48109, USA.*

[§] These authors contributed equally to this work.
[*] Corresponding author: ajhart@mit.edu

ABSTRACT

Liquid crystalline polymers have recently been engineered to exhibit complex macroscopic shape adaptivity, including optically- and thermally- driven bending, self-sustaining oscillation, torsional motion, and three dimensional folding. Miniaturization of these novel materials is of great interest for both fundamental study of processing conditions and for the development of shape-changing micro-devices. Here, we present a scalable method for high-fidelity replica molding of glassy liquid crystalline polymer networks (LCNs), by vacuum-assisted replica molding, along with magnetic field-induced control of the molecular alignment. We find that an oxygen-free environment is essential to establish high fidelity molding with low surface roughness. Identical arrays of homeotropic and polydomain LCN microstructures are fabricated to assess the influence of molecular alignment on the elastic modulus (E = 1.48 GPa compared to E = 0.54 GPa), and side view imaging is used to quantify the reversible thermal actuation of individual LCN micropillars by high-resolution tracking of edge motion. The methods and results from this study will be synergistic with future advances in liquid crystalline polymer chemistry, and could enable the scalable manufacturing of stimuli-responsive surfaces for applications including microfluidics, tunable optics, and surfaces with switchable wetting and adhesion.

KEYWORDS: liquid crystal polymer, microstructures, replica molding, actuation, surfaces

1. INTRODUCTION

Liquid crystalline polymers are rapidly emerging as a platform for the design and manufacturing of stimuli-responsive materials.[1] Incorporation of liquid crystalline moieties within crosslinked polymers[2], along with local and global manipulation of the nematic director, enables liquid crystalline polymers to exhibit complex macroscopic shape adaptivity. As a result, liquid crystalline polymers have been fabricated into structures having optically- and thermally- driven bending,[3] self-sustaining oscillation,[4] torsional motion,[5-8] and three dimensional folding.[2]

However, while extensive studies of LC materials have been performed at millimeter-scale and larger dimensions, fewer studies exist on microstructured liquid crystalline polymers.[9-17] This is arguably due to the difficulty of manufacturing high-fidelity features at microscale simultaneously while controlling the molecular orientation that is critical to maximizing the active properties of the polymer network. Formation and shaping of liquid crystalline polymers in miniaturized formats is of great interest for applications including microfluidics, tunable optics, mechanical metamaterials, and surfaces with switchable wetting and adhesion.

Molding methods are arguably the most suitable and scalable means to bridge this gap, because of the combination of shape versatility, feature resolution, and surface quality that can be achieved by molding. While replica molding of microstructures using master templates has been widely applied to conventional microfabrication polymers, replica molding of liquid crystalline elastomer (LCE) micropillars has exhibited rather poor fidelity (e.g., edge quality and sharpness), rough surfaces, and limited control of geometry and aspect ratio.[18] In addition, studies of liquid crystalline polymer microstructures have been primarily focused on generating large strain responses using soft LCEs, while there has not been extensive study of glassy liquid crystalline polymer network (LCN) microstructures that have higher stiffness at the expense of lower strain response. In order to advance applications of liquid crystal network polymers in active surfaces, and to understand how microscale confinement influences network organization and active behavior, robust fabrication processes for microstructured surfaces are needed for both LCEs and LCNs.

We report the use of replica molding to fabricate high-fidelity microstructures of a model liquid crystalline polymer network (LCN). This is enabled using a custom-built apparatus wherein the LCN microstructures are formed under controlled atmosphere, temperature, light exposure, and magnetic field. We show that atmosphere control is essential to achieve the high-fidelity replica molding, and demonstrate that application of the magnetic field during curing establishes homeotropic order and mechanical anisotropy, which are characterized by polarized microscopy and nanoindentation, respectively. Finally, we quantify the reversible thermal actuation behavior of homeotropic and polydomain microstructures using high-resolution optical imaging.

2. METHODS

To facilitate replica molding of LCN microstructures, silicon master microstructures (Fig. 1c, left) of various cross-sectional shapes with feature sizes ranging from 10 μm to 300 μm and an approximate height of 80 μm were fabricated by photolithography and deep reactive ion etching (DRIE). Soft lithography was then employed to cast a PDMS negative mold (cured at 80 °C for 3 hours) from the silicon microstructures. Prior to casting, the silicon master surface was treated with a hydrophobic coating (tridecafluoro-1,1,2,2,-tetrahydrooctyl)-trichlorosilane to facilitate separation of the silicon master and the PDMS.

The liquid crystal polymer network (LCN) was synthesized from a mixture of reactive liquid crystalline monomers 78.5 wt% RM 257 (Merck), 20 wt% 2-azo (BEAM Co.) and 1.5 wt% photoinitiator I-784 (Ciba) via photopolymerization. The chemical structures of the mixture are shown in Figure S1 in the Supporting Information.

The powders of the above chemicals were mechanically mixed prior to heating on a glass slide placed onto a hotplate set at 120 °C for ca. 3 minutes. Then the PDMS negative mold (ca. 2 cm x 1 cm) was placed on top of the molten mixture. The PDMS mold was gently pressed on the molten mixture to facilitate the filling process. After 2 minutes, the sample was transferred to a preheated (75 °C) stage (Figure 1b) inside a vacuum chamber (Figure S2). This temperature is slightly above the nematic to isotropic transition temperature of the mixture used. The temperature and duration of the mixture on the hotplate for melting are critical process parameters. We found that using a hotplate temperature 120 °C temperature and/or a time longer than 5 minutes would cause thermal curing of the mixture, which would undesirably fix the random molecular orientation of the network before alignment and photocuring.

The custom-built LCN curing apparatus was critical to achieve the results reported in this study. The stage inside the vacuum chamber was composed of a silicon wafer piece with a thin film heater (BK3552, BIRK) thermally bonded to its backside, attached to a modified section of rectangular fused quartz tube. The two ends of the silicon piece were clamped in the quartz stage, suspended over a recess, where an NdFeB rare earth magnet (BX088SH, K&J Magnetics) was optionally placed. The magnetic field is therefore oriented vertically with a measured strength of approximately 0.4 T, which is critical to establish homeotropic alignment of the LCNs. After the molten LCN sample was loaded on the stage the chamber was evacuated to 10 Torr. A degassing step was performed by repeating a venting-pumping procedure three times. After allowing the sample to equilibrate for 8 minutes at 75 °C, the mixture was photopolymerized by exposure to a green light emitting diode (LED) source (60 mW/cm^2, 540 nm) for 1 hour while keeping the substrate at 75 °C. The sample was then cooled to room temperature and the microstructured LCN material was manually delaminated from the PDMS mold. For replica molding of polydomain LCNs, the identical procedure was performed except that the magnet was removed from the quartz stage.

In addition to LCN microstructures, LCN films were also fabricated by filling glass cells enclosed by two glass slides separated by micro glass rods (Nippon Electric Glass Co. Ltd), which established the film thickness. LCN films were utilized for POM, FT-IR, and nanoindentation measurements.

The elastic moduli of polydomain and homeotropic LCNs were measured by nanoindentation (TI900, Hysitron). A sharp sapphire indenter with 1 μm diameter at the tip was indented on five different locations of each film to a maximum depth of 500 nm at a 10 nm/s of indentation rate and 3 seconds of stoppage between loading and unloading. The surface moduli were determined from the unloading curves by the Oliver-Pharr method.

The optical system used to image thermal actuation of the LCN microstructures comprised a 20X objective (NT46-145, Edmund Optics) and a 16X zoom tube lens (NT56-219, Edmund Optics), connected to a high resolution digital camera (Nikon D5100). The LCN sample was placed on a metal ceramic heater (HT24S, Thorlabs) controlled by a temperature controller (PTC 10, Stanford Research Systems).

3. RESULTS

3.1 High fidelity replica molding of LCN microstructures

High-fidelity replica molding of arrays of LCN microstructures was achieved by replica molding. For this, it was essential to accurately mix and carefully heat the precursor mixture to achieve an amorphous melt that fills the PDMS mold, followed by photocuring in an oxygen-free environment. For replica molding under controlled atmosphere, a custom apparatus was constructed as described in the Methods section. In Figure 1c, we show exemplary arrays of LCN microstructures that were fabricated on glass substrates using the replica molding technique. These include structures with varied cross-sectional shapes and smooth vertical sidewalls matching the master template, high aspect ratios (e.g., a small as 10 μm diameter, ca. 80 μm height), and sharp corners (< 2 μm corner radius).

The fidelity of the molding process was evaluated by comparing the height (Dektak XT^{TM}, Bruker with 2 μm stylus radius) of the silicon master with its LCN replica. A typical line scan result in Figure S3 shows heights of 80.37 μm and 79.33 μm of the microstructures (an 'M' shape) on the silicon master and the LCN sample, respectively. This small difference in measured heights (1.29%) indicates full filling of the liquid crystal mixture into the PDMS negative mold.

Moreover, the vacuum environment during the LCN molding process is critical for degassing the molten monomer mixture and for complete filling of the molten mixture into the microcavities of the PDMS mold. LCNs prepared by the same procedure without evacuating the chamber resulted in void formation (Figure 2a) and large surface roughness, due to trapped air bubbles within the LCN mixture. In Figure 2b, we show a sample that was degassed yet exposed to air during polymerization. Here, the roughness is much higher near the exposed edge. Degassed samples that were exposed to nitrogen during polymerization (not shown) retained the high fidelity surfaces of the master mold. Therefore, we conclude that oxygen exposure is deleterious to the surface quality of the LCN replica, likely due to oxygen-induced degradation of the polymer at elevated temperature prior to curing. The presence of both oxygen and moisture can scavenge free radicals, reducing the degree of polymerization and molecular weight, and causing more defect formation through side reactions. We believe that removal of oxygen is more important in our case since the processing temperature is as high as 120 °C for homogenization and 75 °C for photopolymerization.

3.2 Control of LCN molecular order

Building from this baseline process, we studied the influence of a magnetic field to control the alignment of the LCN before and during the curing step, whereby the rod-like mesogens of liquid crystalline monomers are known to orient along the magnetic field.[19] Thus, the average direction of the molecular long axes in the liquid crystalline network, referred to as the nematic director, can be controlled by the direction of the external magnetic field. The orientation of the LCN director was characterized by polarized optical microscopy (POM) (Axioskop 50, Carl Zeiss) at ambient conditions after finishing the fabrication process.

POM images of LCN films (10 μm thick) and microstructures fabricated with homeotropic and polydomain order (i.e., with and without the magnet present during the curing step) are compared in Figure 3a. Polydomain LCN films and micropillar arrays appear bright under crossed polarizers (referred to as polarizer and analyzer) regardless of sample rotation, indicating the birefringent nature of the randomly oriented anisotropic liquid crystalline molecules. For homeotropic LCN films and microstructures the images are dark (Figure S4), regardless of the orientation of the sample under the

optics, suggesting molecular alignment orthogonal to the crossed polarizers (parallel to the sample thickness direction). An SEM image of the microstructures corresponding to these optical images is shown in Figure S5.

The influence of magnetically-induced alignment is further characterized by comparing the mechanical properties of polydomain and homeotropic LCNs. Nanoindentation was performed on LCN films (~10 μm thick), as shown in Figure 3. A greater elastic modulus is expected in the parallel direction to the nematic director in polymer networks while the lowest modulus is indicative of the perpendicular direction to the nematic director.[20] Thus, the homeotropic film, whose director is perpendicular to the film surface, should exhibit a higher elastic modulus compared to the randomly oriented polydomain film. As expected, the homogeneous molecular orientation along the applied load resulted in threefold increase in elastic modulus (1.48 GPa) in comparison with the random molecular orientation of the polydomain film (0.54 GPa). The ratio of standard deviation to the average provides the coefficient of variation (CV). A very low CV value (CV=0.03) is measured from the homeotropic film while a relatively large CV (CV=0.23) value is found from the randomly aligned polydomain film. The identical FT-IR spectra (Figure S6) confirm the same chemical composition of both homeotropic and polydomain LCNs and illustrates that different mechanical properties arise solely from molecular alignment.

3.3 Thermal actuation of LCN microstructures

Aligned liquid crystalline polymers have maximum expansion perpendicular to the nematic director and largest contraction parallel to the nematic director upon heating.[21] To investigate this for the molded microstructures, the temperature-induced actuation response of the LCN microstructures was studied by in-situ optical imaging as illustrated in Figure 4a. Side-view observation was chosen to enable observation of the effects of the substrate constraint on the shape change.

Figure 4 demonstrates the thermomechanical strain response of a homeotropic LCN micropillar with a diameter of ca. 30 μm. Prior to the analysis, the sample was heated from 30 ºC to 160 ºC and then cooled to 30 ºC to relax residual stress from the curing process. During the first subsequent heating and cooling cycle, the micropillar expanded in its radial direction and contracted in its axial direction (vertical). This anisotropic thermal response is concomitant with a decrease in the order of the network at elevated temperature. [21-23]

This thermomechanical actuation is spontaneous upon heating and is fully reversed after cooling. To demonstrate this, seven heating-cooling cycles were examined by cycling from 30 ºC to 160 ºC. An automated edge-tracking algorithm was developed (see Supporting Information) to precisely determine the normalized changes in the pillar height (H) and diameter (D) in microstructures. As shown in Figure 4c and d, the normalized height and diameter values are reversible and repeatable during the actuation cycles, with an average of 1.5% decrease in the pillar height and 3.1% increase in the pillar diameter over the seven actuation cycles. The coefficients of thermal expansion (CTE, α) were calculated along the pillar axial and radial directions at 160 ºC. For the homeotropic LCN micropillar, the average CTE parallel to the axial direction, which is also parallel to the molecular director, is -113 ppm/ºC (negative CTE for contraction) at 160 ºC over the seven cycles. The CTE orthogonal to the director (parallel to pillar radial direction) is 241 ppm/ºC. These values are close to those of previous reports using similar crosslinked LCN materials in the form of films. [20-23]

The thermomechanical behavior of a polydomain LCN microstructure was also characterized (see Figure S7). As expected, a relatively isotropic thermal expansion occurred for both height and diameter upon heating because of the random molecular orientation in the polydomain networks. Here, the increase in the average normalized height and the diameter is 3.64% and 1.79%, which corresponds to CTE of 280

ppm/ºC and 138 ppm/ºC, respectively. The smaller thermal expansion in diameter can be explained by the substrate constraint, as the heated pillar appears 'barrel' shaped in the side view images. Comparing the thermal actuation results of the homeotropic and the polydomain micropillars, it is clear that anisotropy in thermal actuation strongly depends on the molecular alignment of the network; the magnetic field induced homeotropic order in the network leads to contraction parallel to the director and expansion perpendicular to it.

By the same method, we examined the thermal actuation of higher aspect ratio micropillars, including the 10 μm diameter homeotropic pillar (height = 80 μm; AR = 8) as shown in Figure S8. This pillar noticeably shrinks in the vertical direction upon heating, as expected. However, due to the smaller scale, and the related challenge of imaging the structures from the side view while attached to the substrate, it was difficult to precisely quantify the percent strain. Nevertheless, this measurement verified the stability of the smaller structures and that their active behavior was preserved.

It is important to note that such highly crosslinked LCN materials do not undergo a nematic to isotropic transition[23] unlike LCEs.[9, 24-25] In other words, thermal degradation of the chemical composition occurs before thermal energy becomes large enough to disturb alignment of liquid crystal into the randomly oriented state. Hence, thermal actuation of LCN relies on glass transition temperature with concert of order parameter decreases not complete disappearance of order like T_{NI}. This different actuation mechanism inherently limits the strain response in LCN chemistry compared to LCEs.

4. DISCUSSION

Despite the high fidelity replica molding and orientation control we have achieved with LCN microstructures, limitations of this fabrication technique must be noted. First, it is challenging to fabricate structures with smaller feature size (<10 μm diameter) and very high aspect ratio (> 10), because of the difficulty of removing the PDMS mold off the LCN sample without damaging the microstructures. As the aspect ratio of the microstructures becomes greater, it is easier for the adhesion force between the PDMS mold and the LCN microstructures to exceed the LCN material strength due to the increased sidewall area relative to the cross-section area of the microstructures. One potential solution is to chemically treat the PDMS mold to reduce the adhesion between the LCN surfaces and the mold therefore facilitate demolding. Another limit is that this technique can only be used to make structures with fixed cross-sectional shapes (structures from extruding 2-D shapes), while complex 3-D structures could be more attractive for applications of active surfaces. Nevertheless, this technique presents a useful way for uniform and high fidelity molding of microstructures, together with detailed characterization of how microstructures influence mechanical responses. Moreover, the method could be extended to other chemistries such as for liquid crystal elastomers (LCEs) and provides a general approach for micromolding of soft materials in combination with both photo- and thermally-controlled curing. With delicate molecular engineering[26] along with scalable shaping techniques, it should be possible to select the stress and strain response of active microdevices and surfaces based on LCEs and/or LCNs.

5. CONCLUSION

In summary, we have presented a scalable replica molding method for LCN microstructures, demonstrating control of the molecular order within the network along with high-fidelity shape control. A nearly identical match is found between the silicon master mold and the LCN microstructures, via the PDMS negative template. The custom built apparatus enables identification of the key features for such process control: vacuum degassing of the molten precursor upon mold infiltration, removal of oxygen from the curing atmosphere, and application of magnetic field and controlled temperature to achieve the final structures. In addition, optical side view imaging enables quantification of the actuation while the structures remain attached to the substrate, which is a critical capability for further work on LC-based active surfaces. Advances in the shape diversity of replica molding using complex microfabricated molds, and optimization of the chemistry to achieve further engineered mechanical response, may potentially enable such surfaces to achieve dynamic modulation of properties such as adhesion, light manipulation, and wetting.

6. ACKNOWLEDGEMENTS

Financial support was provided by the National Institutes of Health (1R21HL114011-01A1) and the Air Force Office of Scientific Research Young Investigator Program (FA9550-11-1-0089). The silicon master molds were fabricated at the Lurie Nanofabrication Facility (LNF) at the University of Michigan. Electron microscopy, polarized optical microscopy, surface profilometry and FT-IR were performed at the MIT Center for Materials Science and Engineering (CMSE). Nanoindentation was performed at the MIT NanoMechanical Technology Laboratory (Nanolab). We thank Timothy J. White at the Air Force Research Laboratory for supplying chemicals and for valuable discussions.

7. REFERENCES

(1) White, T. J.; Broer, D. J. Programmable and Adaptive Mechanics with Liquid Crystal Polymer Networks and Elastomers. *Nat. Mater.* **2015,** *14*, 1087-1098.
(2) Ware, T. H.; McConney, M. E.; Wie, J. J.; Tondiglia, V. P.; White, T. J. Voxelated Liquid Crystal Elastomers. *Science* **2015,** *347*, 982-984.
(3) Yu, Y.; Nakano, M.; Ikeda, T. Photomechanics: Directed Bending of a Polymer Film by Light. *Nature* **2003,** *425*, 145-145.
(4) White, T. J.; Tabiryan, N. V.; Serak, S. V.; Hrozhyk, U. A.; Tondiglia, V. P.; Koerner, H.; Vaia, R. A.; Bunning, T. J. A High Frequency Photodriven Polymer Oscillator. *Soft Matter* **2008,** *4*, 1796-1798.
(5) Sawa, Y.; Ye, F.; Urayama, K.; Takigawa, T.; Gimenez-Pinto, V.; Selinger, R. L. B.; Selinger, J. V. Shape Selection of Twist-Nematic-Elastomer Ribbons. *Proc. Natl. Acad. Sci. U.S.A.* **2011,** *108*, 6364-6368.
(6) Lee, K. M.; Bunning, T. J.; White, T. J. Autonomous, Hands-Free Shape Memory in Glassy, Liquid Crystalline Polymer Networks. *Adv. Mater.* **2012,** *24*, 2839-2843.
(7) Wie, J. J.; Lee, K. M.; Smith, M. L.; Vaia, R. A.; White, T. J. Torsional Mechanical Responses in Azobenzene Functionalized Liquid Crystalline Polymer Networks. *Soft Matter* **2013,** *9*, 9303-9310.

(8) Iamsaard, S.; Asshoff, S. J.; Matt, B.; Kudernac, T.; Cornelissen, J. J. L. M.; Fletcher, S. P.; Katsonis, N. Conversion of Light into Macroscopic Helical Motion. *Nat. Chem.* **2014,** *6*, 229-235.
(9) Buguin, A.; Li, M.-H.; Silberzan, P.; Ladoux, B.; Keller, P. Micro-Actuators: When Artificial Muscles Made of Nematic Liquid Crystal Elastomers Meet Soft Lithography. *J. Am. Chem. Soc.* **2006,** *128*, 1088-1089.
(10) van Oosten, C. L.; Bastiaansen, C. W. M.; Broer, D. J. Printed Artificial Cilia from Liquid-Crystal Network Actuators Modularly Driven by Light. *Nat. Mater.* **2009,** *8*, 677-682.
(11) Ohm, C.; Kapernaum, N.; Nonnenmacher, D.; Giesselmann, F.; Serra, C.; Zentel, R. Microfluidic Synthesis of Highly Shape-Anisotropic Particles from Liquid Crystalline Elastomers with Defined Director Field Configurations. *J. Am. Chem. Soc.* **2011,** *133*, 5305-5311.
(12) Yan, Z.; Ji, X.; Wu, W.; Wei, J.; Yu, Y. Light-Switchable Behavior of a Microarray of Azobenzene Liquid Crystal Polymer Induced by Photodeformation. *Macromol. Rapid Commun.* **2012,** *33*, 1362-1367.
(13) Wei, R.; Zho, L.; He, Y.; Wang, X.; Keller, P. Effect of Molecular Parameters on Thermomechanical Behavior of Side-on Nematic Liquid Crystal Elastomers. *Polymer* **2013,** *54*, 5321-5329.
(14) Wu, Z. L.; Wei, R.; Buguin, A.; Taulemesse, J. M.; Le Moigne, N.; Bergeret, A.; Wang, X.; Keller, P. Stimuli-Responsive Topological Change of Microstructured Surfaces and the Resultant Variations of Wetting Properties. *ACS Appl. Mater. Interfaces* **2013,** *5*, 7485-7491.
(15) Liu, X.; Wei, R.; Hoang, P. T.; Wang, X.; Liu, T.; Keller, P. Reversible and Rapid Laser Actuation of Liquid Crystalline Elastomer Micropillars with Inclusion of Gold Nanoparticles. *Adv. Funct. Mater.* **2015,** *25*, 3022-3032.
(16) Cui, J.; Drotlef, D.-M.; Larraza, I.; Fernandez-Blazquez, J. P.; Boesel, L. F.; Ohm, C.; Mezger, M.; Zentel, R.; del Campo, A. Bioinspired Actuated Adhesive Patterns of Liquid Crystalline Elastomers. *Adv. Mater.* **2012,** *24*, 4601-4604.
(17) Torras, N.; Zinoviev, K. E.; Esteve, J.; Sanchez-Ferrer, A. Liquid-Crystalline Elastomer Micropillar Array for Haptic Actuation. *J. Mater. Chem. C* **2013,** *1*, 5183-5190.
(18) Wu, Z. L.; Buguin, A.; Yang, H.; Taulemesse, J.-M.; Le Moigne, N.; Bergeret, A.; Wang, X.; Keller, P. Microstructured Nematic Liquid Crystalline Elastomer Surfaces with Switchable Wetting Properties. *Adv. Funct. Mater.* **2013,** *23*, 3070-3076.
(19) de Gennes, P. G.; Prost, J. *The Physics of Liquid Crystals*. Oxford University Press: New York, 1995; Chapter 3, pp 117-118.
(20) van Oosten, C. L.; Harris, K. D.; Bastiaansen, C. W.; Broer, D. J. Glassy Photomechanical Liquid-Crystal Network Actuators for Microscale Devices. *Eur. Phys. J. E. Soft Matter* **2007,** *23*, 329-336.
(21) Mol, G. N.; Harris, K. D.; Bastiaansen, C. W. M.; Broer, D. J. Thermo-Mechanical Responses of Liquid-Crystal Networks with a Splayed Molecular Organization. *Adv. Funct. Mater.* **2005,** *15*, 1155-1159.
(22) Broer, D. J.; Mol, G. N. Anisotropic Thermal-Expansion of Densely Cross-Linked Oriented Polymer Networks. *Polym. Eng. Sci.* **1991,** *31*, 625-631.
(23) Wie, J. J.; Lee, K. M.; Ware, T. H.; White, T. J. Twists and Turns in Glassy, Liquid Crystalline Polymer Networks. *Macromolecules* **2015,** *48*, 1087-1092.
(24) Warner, M.; Terentjev, E. M. *Liquid Crystal Elastomers*. Oxford University Press: New York, 2003; Chapter 2, pp 15-20.
(25) deGennes, P. G.; Hebert, M.; Kant, R. Artificial Muscles Based on Nematic Gels. *Macromol. Symp.* **1997,** *113*, 39-49.

(26) Wie, J. J.; Wang, D. H.; Lee, K. M.; Tan, L.-S.; White, T. J. Molecular Engineering of Azobenzene-Functionalized Polyimides to Enhance Both Photomechanical Work and Motion. *Chem. Mater.* **2014,** *26*, 5223-5230.

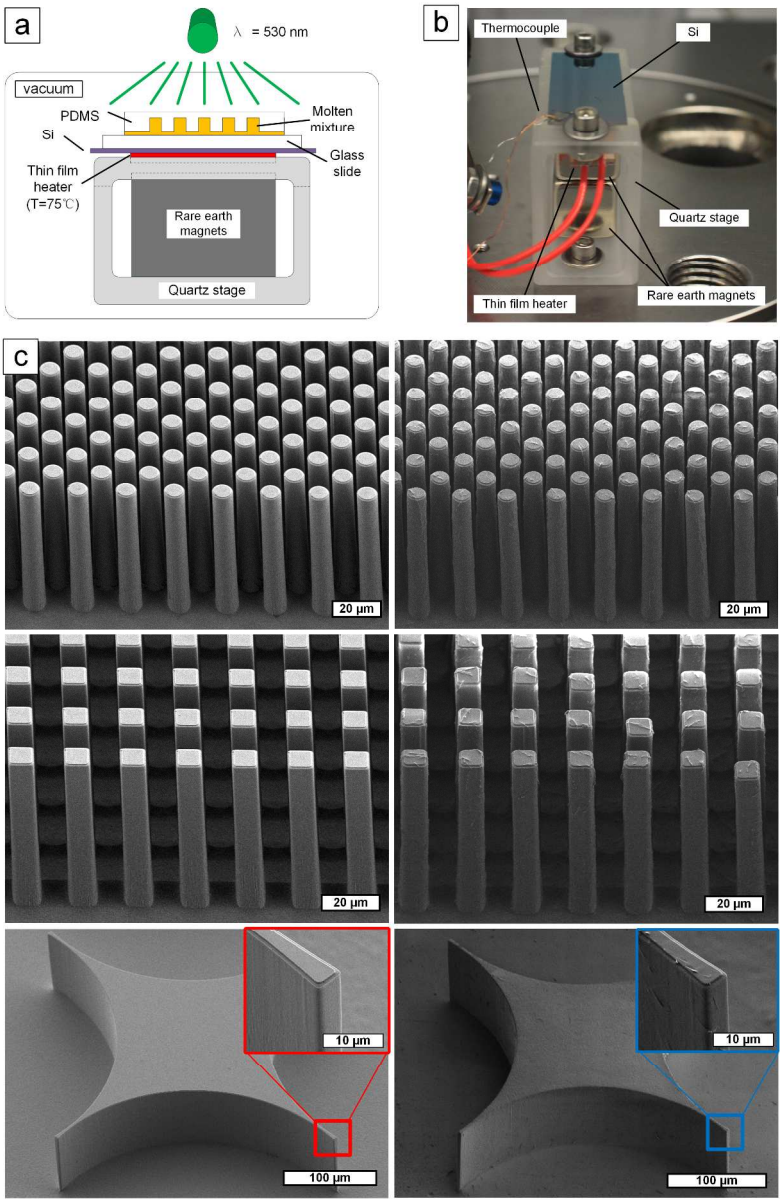

Figure 1. (a) Schematic of the experimental setup for replica molding of homeotropic LCN microstructures (complete system shown in Fig. S2). (b) Heated stage assembly with magnets inserted. (c) SEM images of the silicon molds (left) and replicated homeotropic LCN microstructures (right), showing large arrays of high aspect ratio micropillars with circular and square cross-sectional shapes, and microstructures with sharp corners.
224x345mm (300 x 300 DPI)

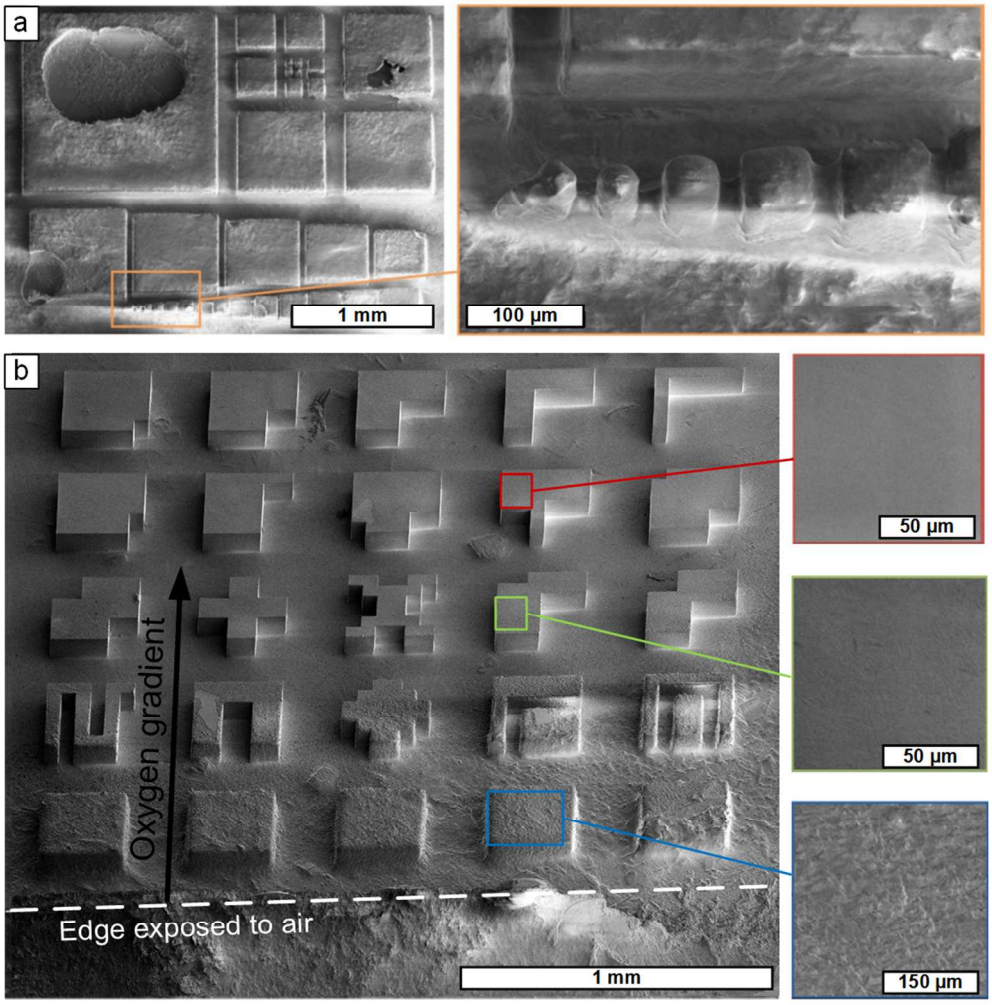

Figure 2. Deleterious influence of oxygen on fidelity and surface roughness of LCN microstructures made by replica molding. (a) LCN replicas fabricated without vacuum degassing of the molten liquid crystalline mixture inside the chamber; (b) LCN replica that was exposed to air during curing, after vacuum degassing. Close-up images show how surface topography varies with distance from the edge of the mold, where oxygen exposure was greatest.
147x151mm (200 x 200 DPI)

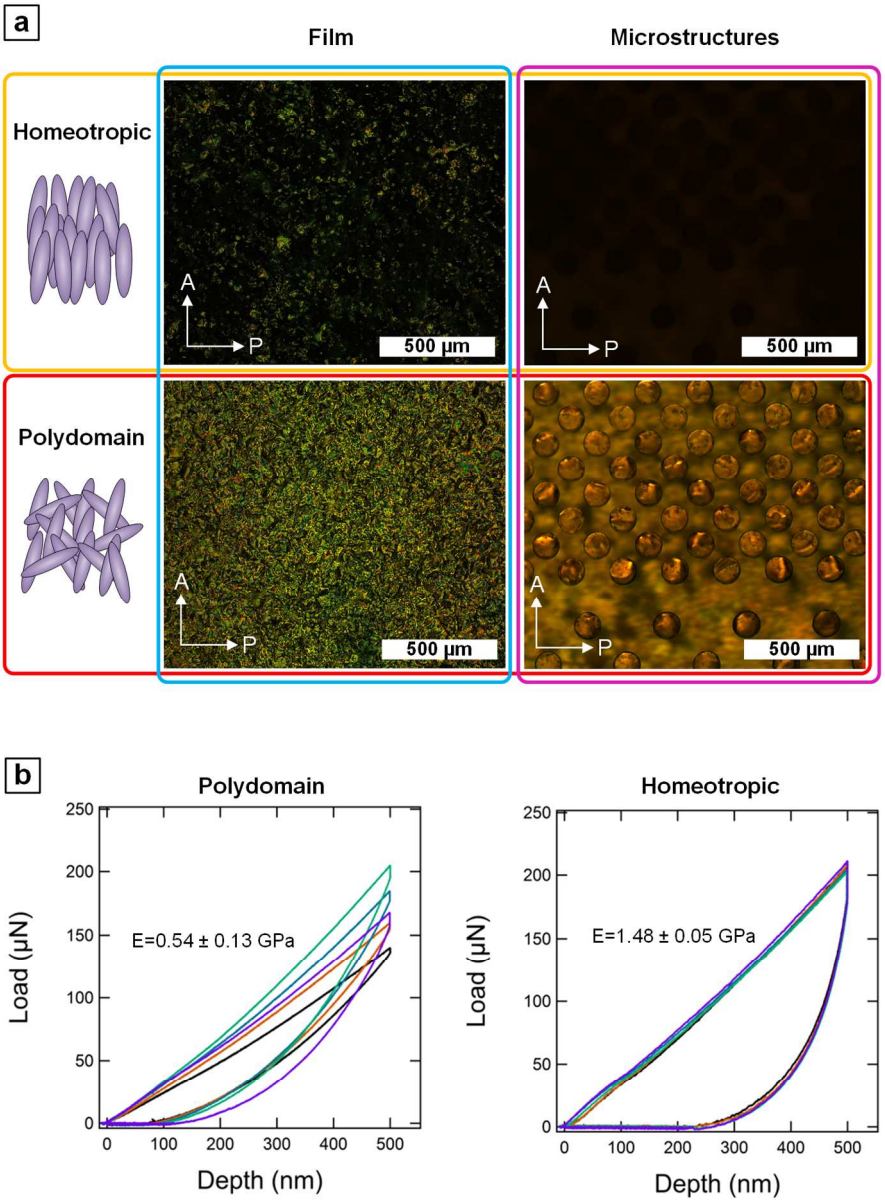

Figure 3. (a) POM micrographs of LCN thin films (10 μm thick) and microstructure arrays with homeotropic and polydomain order; (b) Loading/unloading curves of polydomain and homeotropic LCN films (10 μm thick) measured by nanoindentation using a 1 μm diameter sized sapphire tip. The elastic modulus is determined by averaging the five nanoindentation measurements from different locations on the film.

194x263mm (200 x 200 DPI)

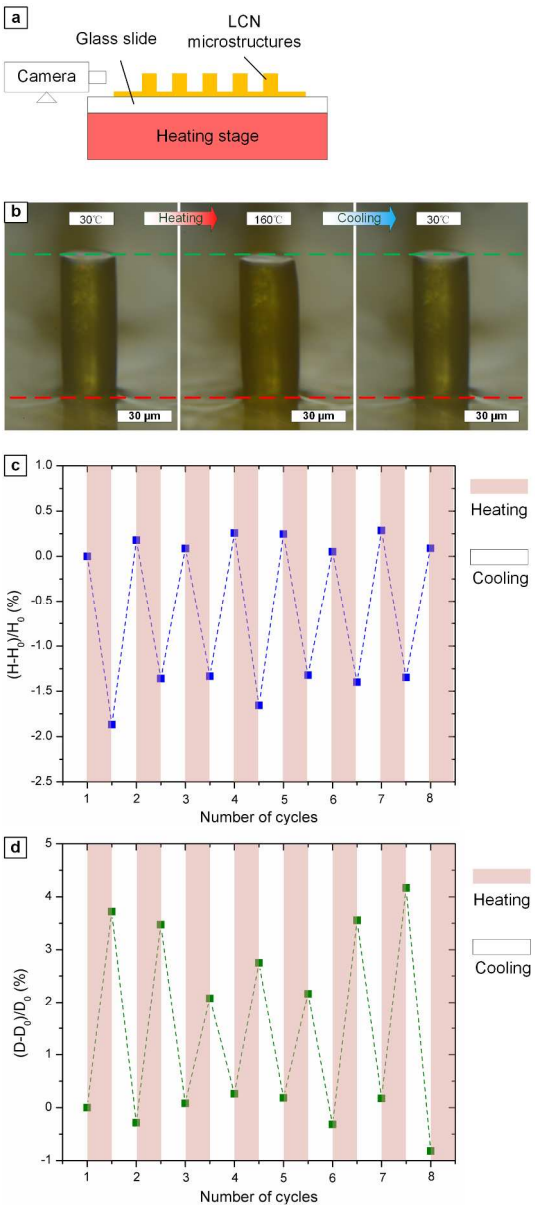

Figure 4. Thermal actuation of homeotropic LCN micropillar within an array. (a) Schematic illustration of the side-view imaging configuration with the micropillar on heated substrate; (b) Side view of a 30 μm diameter homeotropic LCN pillar during heating and cooling. The three images are aligned at the base of the micropillar (indicated by the red dotted line near the bottom). The green dotted line near the top of the micropillar is aligned with the top surface of the micropillar in the left image (30 ºC). Normalized (c) height and (d) diameter changes of the LCN micropillar during heating (to 160 ºC) and cooling (to 30 ºC) cycles measured using image processing based on an edge tracking algorithm.
205x458mm (200 x 200 DPI)

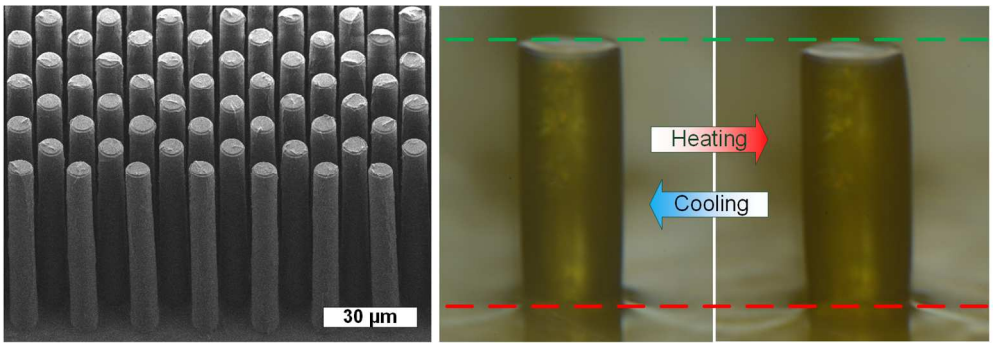

221x74mm (200 x 200 DPI)